

# **A facile single-step procedure for the synthesis of luminescent Ln<sup>3+</sup>:YVO<sub>4</sub> (Ln = Eu or Er + Yb)-silica nanocomposites**

Manuel Ocaña (a); Eugenio Cantelar (b); Fernando Cussó (b)

(a) Instituto de Ciencia de Materiales de Sevilla, CSIC-US, Américo Vespucio 49, 41092 Isla de la Cartuja, Sevilla, Spain

(b) Depto. Física de Materiales, C-IV, Universidad Autónoma de Madrid, Spain

## **Abstract**

A simple and single-step method for the production of Ln-doped YVO<sub>4</sub> nanocrystals and their simultaneous encapsulation in a silica network based on the pyrolysis of liquid aerosols at 800 ° C is reported. The procedure is illustrated for Yb,Er:YVO<sub>4</sub>-silica nanocomposites consisting of spherical particles, which present up-converted green luminescence after IR excitation whose efficiency increased on annealing up to 1000 ° C due to the release of impurities (adsorbed water, and residual anions). XPS spectroscopy and TEM observations revealed that the surface of the composite particles was enriched in silica, which would facilitate their functionalisation required to use them in biological applications. The procedure can also be used to prepare other rare earth doped systems as illustrated for the case of Eu-doped YVO<sub>4</sub>/silica having down-converted red luminescence.

## **Keywords :**

Nanocomposites; Yttrium orthovanadate; Silica; Europium; Erbium; Ytterbium

## **1. Introduction**

Recently, lanthanide-based nanoparticles consisting of different matrices (lanthanide fluorides, phosphates or orthovanadates) doped with lanthanide (Ln) ions have gained popularity as luminescent materials for many biomedical applications (biolabelling [1], drug delivery [2] and sensing [3]), since they present several advantages when compared with other fluorescent systems (organic dyes, quantum dots). To mention a few, the emission bands of the luminescent cations are narrower than those of dyes or quantum dots thus increasing the assays sensitivity, the toxicity of these lanthanide materials is also lower than that of the other luminescent compounds and finally, when co-doping with Yb and Er or Tm, the lanthanide systems present up-conversion luminescence, i.e., visible emission after excitation with infrared (IR) radiation. This property is very convenient for bioapplications since IR radiation does not damage biological tissues.

It has been shown that for most of the above mentioned applications, it is beneficial to deposit silica shells onto the lanthanide-based nanoparticles to facilitate bioconjugation with biological molecules [4], [5] and [6] or to prevent exposure of lanthanide ions to living tissues [5]. Moreover, it has been reported that the efficiency of the Ln emission processes and photostability may be also improved by the silica layer, which minimises the quenching of the excited states in the Ln cations located on the nanoparticles surface through interaction with surface OH groups [7] and [8]. Usually, these lanthanide nanophosphors-silica composites are prepared by different liquid phase procedures [4], [5] and [6], which involve an initial synthesis and purification of the luminescent nanoparticles and in a second stage, the surface precipitation of the silica layers.

In this work, we report a simple and single-step method for the production of Ln-doped YVO<sub>4</sub> nanocrystals and their simultaneous encapsulation in a silica network. This procedure is based on the pyrolysis of liquid aerosols generated from solutions of appropriated Ln precursors and TEOS using a water:ethanol mixture as solvent. This procedure is illustrated for up-converting Yb,Er:YVO<sub>4</sub>-silica composites, whose luminescent properties are studied in detail. In order to elucidate the localisation of the Ln ions in the resulting composites, a Eu:YVO<sub>4</sub>/silica sample was previously synthesised by the same procedure, since the Eu<sup>3+</sup> emission properties are sensitive to the Eu<sup>3+</sup> cations environment so that they can be used as a probe of the dopants localisation in the luminescent nanocomposites [9].

## 2. Experimental

### 2.1. Particle synthesis

Tetraethyl orthosilicate (TEOS, Fluka, >98%), vanadyl sulfate (VOSO<sub>4</sub>· 4H<sub>2</sub>O, Aldrich, 97%), yttrium chloride (YCl<sub>3</sub>· 6H<sub>2</sub>O, Aldrich, >99%), europium chloride (EuCl<sub>3</sub>· 6H<sub>2</sub>O, Aldrich, >99%), ytterbium chloride (YbCl<sub>3</sub>· 6H<sub>2</sub>O, Aldrich, 99.9%) and erbium chloride (ErCl<sub>3</sub>· 6H<sub>2</sub>O, Aldrich, 99.9%) were used as received.

The lanthanide nanophosphors-silica composites were prepared by pyrolysis of liquid aerosols in an apparatus previously described [10], according to the following procedure. The starting solutions (250 cm<sup>3</sup>) were prepared by dissolving in a mixture ethanol/water (50/50 volumetric ratio) equimolecular amounts (0.05 mol dm<sup>-3</sup>) of TEOS and vanadyl sulphate and proper amounts of lanthanide chlorides to achieve the desired compositions (Eu<sub>0.05</sub>Y<sub>0.95</sub>VO<sub>4</sub> and Er<sub>0.02</sub>Yb<sub>0.1</sub>Y<sub>0.88</sub>VO<sub>4</sub>). The use of ethanol was needed since, as it is well known, TEOS is immiscible with water. The aerosols were generated from these solutions by nebulisation, using a glass nozzle and air at constant pressure (0.5 kg cm<sup>-2</sup>) as a carrier gas. Then, they were introduced into an expansion chamber and transported through two consecutive furnaces kept at 400 and 800 °C, respectively, in which, the liquid droplets were dried and thermally decomposed. The resulting solid particles were finally collected in a glass filter with a very high efficiency and washed with distilled water for purification. For some analyses, the obtained powders were heated for 3 h at different temperatures in platinum crucibles. The furnace containing the samples was heated at 10 °C min<sup>-1</sup> up to the desired temperature.

## 2.2. Characterization

The shape of the nanoparticles was examined by scanning (SEM, Jeol JSM5400) and transmission electron microscopy (TEM, Philips 200CM).

The qualitative composition of the precipitated particles was assessed by energy dispersive X-ray analysis (EDX, Philips DX4) coupled to the TEM microscope.

X-ray photoelectron spectra (XPS) of the samples were measured with a VG Escalab apparatus (Model 210) using the  $AlK\alpha$  excitation source for europium and  $MgK\alpha$  for the rest of elements. Calibration of the spectra was done at the Si 2p peak taken at 103.1 eV. The peaks areas were corrected by the sensitivity factors of the elements as supplied by the instrument manufacturers.

The crystalline structure of the prepared nanoparticles was identified by X-ray diffraction (Siemens D501). The crystallite size was estimated from the most intense XRD peak of the YVO<sub>4</sub> structure ( $2\theta \sim 25^\circ$ ) by using the Scherrer method.

The infrared spectra of the powders diluted in KBr pellets were recorded in a Nicolet 510 Fourier transform spectrometer.

Thermogravimetric analysis (TGA) was performed in air at a heating rate of  $10^\circ \text{C min}^{-1}$ , using a Q600 TA Instrument.

For the Eu-doped system, the excitation and emission spectra of the samples dispersed in water were measured in a Horiba Jobin Yvon spectrofluorimeter (Fluorolog FL3-11) operating with a slit of 1 nm. For the up-converting Yb,Er co-doped system, the optical measurements were performed for powdered pressed samples using a continuous wave (CW) JENOPTIK laser diode source at 980 nm to excite the Yb<sup>3+</sup> ions with different excitation powers. The visible Er<sup>3+</sup> luminescence was dispersed by using an ARC Spectrapro 500-I monochromator and then detected with a photomultiplier tube. In order to achieve reproducible and comparative luminescence spectra, all the data have been taken using a standard experimental arrangement, including specially design sample holders. They were constructed using a 2 mm-thick PMMA spacer with a 3-mm-diameter circular opening, enclosed by two microscope slide covers. The powders were introduced filling the cavity which was placed in a fixed mount on the top of a micrometer stage, in order to optimize the luminescence signal. The diode laser beam was limited by a diaphragm assuring that the excitation area was smaller than the exposed sample area. The sample holder can be removed and replaced into this arrangement without altering the geometry. It has been checked that luminescence spectra are reproducible with integrated intensity variations smaller than 3%. All emission spectra have been corrected for the response of the monochromator grating and photomultiplier tube.

For lifetime measurements, an Optical Parameter Oscillator (Spectra-Physics MOPO-730), with pulse length of 10 ns and a repetition rate of 10 Hz, was used as excitation. The fluorescence was detected with an EMI-9558QB photomultiplier tube and the signal was synchronously averaged and recorded by a digital oscilloscope.

The emission spectra were transformed to the CIE colour coordinates system using the 2° standard observer [11].

### 3. Results and discussion

#### 3.1. *Eu:YVO<sub>4</sub>/silica nanocomposites*

As previously mentioned, we first addressed the synthesis of the down-converting (DC) luminescent Eu:YVO<sub>4</sub>/silica system since the Eu<sup>3+</sup> emission properties are sensitive to the Eu<sup>3+</sup> cations environment [9].

An illustrative SEM picture of sample DC having a nominal SiO<sub>2</sub>/Eu<sub>0.05</sub>Y<sub>0.95</sub>VO<sub>4</sub> molar ratio of 1:1 (Table 1) is shown in Fig. 1. As observed, they consisted of spherical particles of broad size distribution (<7  $\mu$ m) some of which present holes revealing that they were hollow. The observation of the spheres under the TEM microscope revealed dark zones surrounded by a layer with slighter contrast which seems to indicate that the YVO<sub>4</sub> crystallites are encapsulated into a silica matrix (Fig. 1, inset). In order to corroborate this suggestion, this sample was examined by XPS, a well known technique for surface analysis, finding that the atomic Si/V ratio obtained from the XPS spectra was much higher (2.4) than the nominal value (1) (Table 1) confirming that the particles outerlayers were enriched in silica.

The EDX spectrum obtained for several single spheres displayed intense peaks due to Si, Y and V along with a much weaker peak corresponding to Eu (Fig. 2), in agreement with the nominal composition of this sample. XRD revealed that the as prepared spheres contained tetragonal YVO<sub>4</sub> [JCPDS file 16–250] (crystallite size = 26 nm, Table 1) as the only crystalline phase (Fig. 3). It should be mentioned that this is the first report on the direct formation of crystalline Eu:YVO<sub>4</sub> by pyrolysis of aerosols not requiring a further annealing treatment since although the preparation of these phosphors by spray pyrolysis has been recently addressed by Zhou and Lin [12], the as prepared powders needed to be further annealed at 700 °C for crystallization. The presence of amorphous silica in the particles was confirmed by their IR spectra (Fig. 4), which showed two intense bands at 1100 and 475 cm<sup>-1</sup> mainly due to the stretching and bending Si–O vibrations, respectively [13], along with a more intense absorption at 820 cm<sup>-1</sup> corresponding to the V–O vibrations of YVO<sub>4</sub>[14].

The emission spectrum of the Eu:YVO<sub>4</sub>/silica composite spheres was measured using an excitation wavelength ( $\lambda_{exc}$ ) of 325 nm [12]. The obtained spectrum (Fig. 5, top) displayed weak bands at 593, 695 and 702 nm along with two strong bands at 614–617 nm, which caused a strong red luminescence in this sample (see CIE colour coordinates, Fig. 6). These bands have been previously reported for Eu:doped YVO<sub>4</sub> nanoparticles and attributed to the Eu<sup>3+</sup>5D<sub>0</sub>  $\rightarrow$  7F<sub>J</sub> (J = 1, 2 and 4) electronic transitions [15] and [16], which have been detailed in the figure. It should be noted that the emission spectrum of Eu<sup>3+</sup> ions in an amorphous silica matrix [17] consisted of broader bands than those detected for our sample, which manifests that the Eu cations are located within the YVO<sub>4</sub> structure in our sample. This finding was further confirmed by the excitation spectrum of the sample (monitored for an emission wavelength of 698 nm), which consisted of a strong and broad band centred at 310 nm (Fig. 5,

down), due to the absorption of vanadate groups. This indicates that the luminescence of this sample is originated from the optical excitation of the host followed by an energy transfer to the  $\text{Eu}^{3+}$  cations, as previously reported for this system [15].

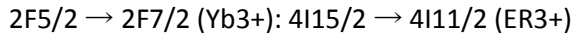
### 3.2. *Er,Yb:YVO4/silica nanocomposites*

UC composites (sample UC) were prepared with a  $\text{SiO}_2/\text{YVO}_4$  molar ratio of 1/1, an  $\text{Er}/\text{Y}$  atomic ratio = 0.02 and a  $\text{Yb}/\text{Y}$  atomic ratio = 0.1. The obtained particles presented similar morphological characteristics and size to those corresponding to the Eu-doped system (sample DC) (Fig. 1). EDX analyses carried out for this sample also confirmed the incorporation of all cations to the spheres in this case (Fig. 2). The XRD pattern (Fig. 3), crystallite size (Table 1) and IR spectra (Fig. 4) of this sample were also similar to those of sample DC indicating that both samples present the same  $\text{YVO}_4$  tetragonal phase.

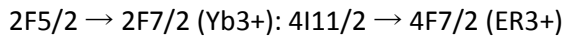
When sample UC was excited with IR radiation ( $\lambda = 980 \text{ nm}$ ), the up-conversion emission bands characteristic of  $\text{Er}^{3+}$ ,  $\text{Yb}^{3+}$  co-doped  $\text{YVO}_4$  nanoparticles [18] were detected whose intensity increased after thermal annealing at increasing temperatures up to  $1000^\circ \text{C}$  (Fig. 7). Such an increase was particularly important for the sample heated at  $1000^\circ \text{C}$  (20 times higher intensity in comparison with the as prepared sample). It should be noted that most particles retained the spherical shape after calcination at  $1000^\circ \text{C}$  (Fig. 8). Particle sintering was detected only at higher temperatures.

The mechanism of up-conversion is well known and can be summarised as follows (Fig. 9). After pumping into the  $\text{Yb}^{3+}$  absorption band ( $2\text{F}_{7/2} \rightarrow 2\text{F}_{5/2}$  transition) at  $\lambda = 980 \text{ nm}$ , the upper multiplets of  $\text{Er}^{3+}$  ions are excited via the up-conversion energy transfers [19], [20], [21] and [22].

(A)



(B)



These processes are very efficient and populate the  $4\text{F}_{7/2}$  level of the  $\text{Er}^{3+}$  ions and, after an intermediate non-radiative relaxation, the  $2\text{H}_{11/2}$  and  $4\text{S}_{3/2}$   $\text{Er}^{3+}$  levels, that decay mainly radiatively to the ground state ( $4\text{I}_{15/2}$  ( $\text{Er}^{3+}$ )), entailing the two dominant green emissions ( $\lambda = 520 \text{ nm}$  and  $540 \text{ nm}$ ) observed in the spectra. A fraction of the excited ions decay also non-radiatively to the  $4\text{F}_{9/2}$  level from where the much weaker emission band in the red spectral region ( $\lambda = 660 \text{ nm}$ ) originates.

The power dependence of the up-conversion luminescence for sample UC, as prepared and heated at different temperatures, is shown in Fig. 10, where the integrated intensity of the  $2\text{H}_{11/2}$ ,  $4\text{S}_{3/2} \rightarrow 4\text{I}_{15/2}$  transitions (green emissions) are plotted as a function of the excitation power. It can be observed that they approximately follow a quadratic dependence ( $m = 2$ ) confirming the mechanism of excitation indicated in equations (A) and (B) that requires the absorption (and transfer) of two excitation photons [23] and [24].

The increase of luminescence intensity with annealing temperature may be related to the improvement of crystallinity and/or the removal of impurities, such as organic species or OH radicals, as it has been reported for different rare-earth doped nanoparticles [25], [26], [27] and [28]. In our case, the XRD pattern remained almost unaltered after calcination (Fig. 3). In fact, the crystallite size estimated from the XRD reflections (Table 1) was only slightly higher for the sample heated at 1000 ° C (~30 nm) than that for the as prepared sample (~26 nm). This unexpected behaviour should be attributed to the silica matrix surrounding the YVO4 grains, which makes difficult the diffusion process required for crystal growth. Therefore, the crystallinity increase does not seem to be the main factor accounting for the considerable increase of luminescence on calcination.

TGA analyses were carried out in order to gain information on the presence of impurities in our sample. The TGA curve measured for sample UC as prepared (Fig. 11) revealed a weight loss of ~3.5% from 25 to 600 ° C followed by a second one of ~2% from 600 to 1000 ° C. The first one, which is mainly ascribed to the release of adsorbed water, might account for the efficiency increase observed after heating the sample at 600 ° C. EDX spectroscopy offered information on the origin of the second weight loss, which should be related to the more important luminescence increase resulting on calcination at 1000 ° C. Thus, the EDX spectrum of the as prepared sample displayed a sulphur peak along with a weaker one due to chlorine, coming from some unreacted sulphate and chloride anions, respectively, whose intensity decreased after annealing at 1000 ° C (Fig. 2). The decomposition of these species would explain, at least in part, the weight loss detected at 600–1000 ° C. Nevertheless, the presence in the sample of some OH groups strongly bonded to the Er,Yb:YVO4 nanocrystals or the silica matrix after calcination at 600 ° C cannot be disregarded.

It should be noted that the annealing treatments also affect the relative intensity of the red and green emissions. From the emission spectra presented in Fig. 7, it was found that the green to red intensity ratio (GRR) of sample UC as prepared was similar to the value obtained after annealing at 600 ° C (GRR = 6.5), while it increased to GRR = 11 after a further heating at 1000 ° C, resulting in an enhanced green emission (Fig. 6). This behaviour might be explained by the same reasons responsible for the intensity increase [25], [26], [27], [28], [29], [30], [31] and [32], and related to a reduction in the efficiency of the non-radiative channels that populate the 4F9/2 (Er3+) level upon calcination, and therefore, in an enhanced luminescence efficiency of the green emissions.

In order to confirm this assumption, the decay of the Er3+ green emission under direct excitation to the emitting multiplets at  $\lambda$  excitation = 520 nm and measured at  $\lambda$  emission = 550 nm, has been also investigated. The results obtained are presented in Fig. 12. It can be observed that either the as prepared sample or after annealing at 600 ° C, exhibit monoexponential decays with characteristic times  $\tau_1 = 2.3 \mu s$  and  $\tau_1 = 2.0 \mu s$ , respectively, while the decay curve measured after annealing at 1000 ° C is non-exponential and it can be fitted as the superposition of two components with lifetimes  $\tau_1 = 2.9 \mu s$  and  $\tau_2 = 13.8 \mu s$ . It should be noted that all samples have been excited and the luminescence collected in a similar geometry, so that the difference in the relative intensities reflect a higher luminescent efficiency for the samples annealed at 1000 ° C, in accordance with the

continuous wave results previously presented. Therefore, the possibility of additional longer components for the less intense emissions detected for sample UC as prepared and heated at 600 ° C cannot be completely discarded, as they would become unobservable due to the lower intensities when compared to those of the sample annealed at 1000 ° C, and only the dominant short components are detected.

We must indicate that the lifetime of the long component decay of the sample annealed at 1000 ° C ( $\tau_2 = 13.8 \mu s$ ) is close to the lifetime reported [34], [35] and [36] for lightly doped samples ( $\tau = 10\text{--}12 \mu s$ ). This component could be then associated to the decay of isolated ions, not affected by cross-relaxation or transfer channels, reflecting therefore the intrinsic lifetime of the green emitting levels. It should be beard in mind that the 2H11/2 and 4S3/2 Er<sup>3+</sup> levels are sufficiently close in energy so that they are thermally coupled (see Fig. 9) and the two levels will decay with a common effective lifetime. The radiative lifetime, calculated from Judd–Ofelt parameters [33] and [34] is  $\tau_{rad} = 112 \mu s$  and the difference with the measured lifetime could be explained on the basis of multiphonon decay to the lower lying 4F9/2 manifold. Therefore, the luminescent quantum efficiency of the (2H11/2, 4S3/2) emitting levels for isolated Er<sup>3+</sup> ions in YVO<sub>4</sub> would be:  $\phi = \tau \exp / \tau_{rad} \approx 10\%$ .

More interesting are the short components of the luminescence decay, which are dominant. As above mentioned, they are of the order of a few microseconds ( $2 \mu s < \tau_1 < 3 \mu s$ ) indicating that they are affected by additional decay channels. In fact, it is well known that Er<sup>3+</sup> ions are very sensitive to concentration quenching due to cross-relaxation processes, and in the case of Er<sup>3+</sup>-doped YVO<sub>4</sub> the characteristic lifetime of the (2H11/2, 4S3/2) green emitting levels is gradually reduced to 9.8  $\mu s$ , 6.6  $\mu s$  and 1.6  $\mu s$  when the concentration increases to 1.0, 2.5 and 10 at% [34], [35] and [36]. In Er<sup>3+</sup>/Yb<sup>3+</sup> co-doped materials, under direct Er<sup>3+</sup> excitation, the transfer between the rare earth ions, may operate also in a back-transfer scheme, with Er<sup>3+</sup> ions acting as donors and Yb<sup>3+</sup> ions as acceptors, as indicated in Fig. 9(b). This mechanism introduces an additional channel for Er<sup>3+</sup> de-excitation, further reducing the corresponding lifetime [37]. It has been reported that for Yb/Er:YVO<sub>4</sub>, with the same Er<sup>3+</sup> content that in the present work, the lifetime of the green emission is reduced to 5  $\mu s$  for the bulk material [4].

The lifetime increase observed on calcination could be due to the elimination of residual impurities (absorbed water and other anions) and involves an increase of the luminescence quantum yield of the (2H11/2, 4S3/2) emitting levels, that can be estimated from the ratio between experimental and radiative (calculated [32] and [33]) lifetimes ( $\phi = \tau \exp / \tau_{rad}$ ). Thus, the variation of lifetime from 2.0  $\mu s$ , for as prepared sample, to 2.9  $\mu s$  after heating at 1000 ° C, represents a change in the luminescent quantum yield from  $\phi \sim 1.8\%$  to  $\phi \sim 2.6\%$  i.e., approximately a 45% increase. It must be mentioned that a substantially shorter lifetime ( $\tau = 0.25 \mu s$ ), and therefore a lower luminescent quantum yield has been reported for other composite silica-YVO<sub>4</sub>:Er,Yb powders consisting of nanoparticles with a mean size of 10 nm [4]. The higher values obtained in our case could be related to the higher crystal size of our nanoparticles (29 nm) and probably, to an efficient encapsulation of the luminescent ions in the silica matrix.

Finally, it is remarkable that all values of the short components of the luminescence decay measured in the present work ( $2 \mu s < \tau_1 < 3 \mu s$ ) are only about a 50% lower than that of the bulk material above mentioned ( $5 \mu s$ ), indicating that the emission properties (lifetime and luminescence efficiency) of our system are very close to those of bulk YVO<sub>4</sub>:Er,Yb.

#### **4. Conclusions**

We have shown that the pyrolysis at 800 ° C of aerosols consisting of solutions (in water/ethanol mixtures) containing TEOS, vanadyl sulphate, yttrium chloride, ytterbium chloride and erbium chloride in appropriated concentrations is able to produce, in a very simple and single-step way, Yb,Er:YVO<sub>4</sub>-silica nanocomposites consisting of spherical particles. These materials present up-converted green luminescence after IR excitation whose efficiency increases when calcined at increasing temperatures (up to 1000 ° C), reaching a final value higher than that found in previous reports. Such an increase is attributed to the release of impurities (adsorbed water, residual sulphate and chloride anions) remaining in the particles after the synthesis process. XPS spectroscopy revealed that in our particles, the surface is enriched in silica, which would facilitate their functionalisation required for their use in biological applications. The procedure can also be used to prepare other rare earth doped systems as illustrated for the case of Eu-doped YVO<sub>4</sub>/silica having down-converted red luminescence.

#### **Acknowledgments**

This work has been funded by the Spanish Ministerio de Ciencia e Innovación (MICINN) (grants MAT2008-02166 and CRONOSOMATSMAT2009-14102) and Junta de Andalucía (grant FQM3579). We also acknowledge Dr. A. Barranco for his assistance in obtaining the DC luminescence measurements.



## References

- [1] D. Giaume, M. Poggi, D. Casanova, G. Mialon, K. Lahlili, A. Alexandru, T. Gacoin, J.P. Boilot  
Langmuir, 24 (2008), p. 11018
- [2] P. Yang, R.S. Huang, D. Kong, J. Lin, H. Fu  
Inorg. Chem., 46 (2007), p. 3203
- [3] L. Wang, R. Yan, Z. Huo, L. Wang, J. Zeng, J. Bao, X. Wang, Q. Peng, Y. Li  
Angew. Chem. Int. Ed., 44 (2005), p. 6054
- [4] V. Buisette, A. Huignard, T. Gacoin, J.P. Boilot, P. Aschehoug, B. Viana  
Surf. Sci., 532–535 (2003), p. 444
- [5] S. Sivakumar, P.R. Diamente, F.C.J.M. van Veggel  
Chem. Eur. J., 12 (2006), p. 5878
- [6] Y. Wang, W. Qin, J. Zhang, C. Cao, J. Zhang, Y. Jin, P. Zhu, G. Wei, G. Wang, L. Wang  
J. Solid State Chem., 180 (2007), p. 2268
- [7] D. Giaume, V. Buisette, K. Lahlil, T. Gacoin, J.P. Boilot, D. Casanova, E. Beaurepaire, M.P. Sauviat, A. Alexandrou  
Prog. Solid State Chem., 33 (2005), p. 99
- [8] Q. Lü, A. Li, F.Y. Guo, L. Sun, L. Zhao  
Nanotechnology, 19 (2008), p. 145701
- [9] H. Meyssamy, K. Riwotzki, A. Kornovski, S. Naused, M. Haase  
Adv. Mater., 11 (1999), p. 840
- [10] E. Lopez-Navarrete, M. Ocaña  
J. Eur. Ceram. Soc., 22 (2002), pp. 353–359
- [11] CIE, Recommendations on Uniform Color Spaces, Color Difference Equations, Psychometrics Color Terms. Supplement No 2 of C.I.E. Publ. No 15 (E1-1.31) 1971. Bureau Central de la CIE, Paris, 1978.
- [12] Y.H. Zhou, J. Lin  
Opt. Mater., 27 (2005), p. 1426

- [13] M. ocaña, V. fornés, C.J. serna  
J. Non-Cryst. Solids, 107 (1989), p. 187
- [14] M. Touboul, M. Popot  
Ann. Rev. Chim. Miner., 22 (1985), p. 610
- [15] K. Riwozki, M. Haase  
J. Phys. Chem. B, 102 (1998), p. 10129
- [16] M. Yu, J. Lin, Z. Wang, J. Fu, S. Wang, H.J. Zhang, Y.C. Han  
Chem. Mater., 14 (2002), p. 2224
- [17] E.W.J.L. Oomen, A.M.A. van Dongen  
J. Non-Cryst. Solids, 111 (1989), p. 205
- [18] T. Tsuboi  
Phys. Rev. B, 62 (2000), p. 4200
- [19] L.F. Johnson, H.J. Guggenheim, T.C. Rich, F.W. Ostermayer  
J. Appl. Phys., 43 (1972), p. 25
- [20] E. Cantelar, F. Cussó  
J. Lumin., 102–103 (2003), p. 525
- [21] F. Vetrone, J.C. Boyer, J.A. Capobianco, A. Speghini, M. Bettinelli  
J. Appl. Phys., 96 (2004), p. 661
- [22] H.X. Mai, Y.W. Zhang, L.D. Sun, C.H. Yan  
J. Phys. Chem. C, 111 (2007), p. 13721
- [23] Y. Kuisheng, Z. Fang, W. Rina, L. Hansheng, Z. Xiyan  
J. Rare Earth., 24 (2006), p. 162
- [24] M. Pollnau, D.R. Gamelin, S.R. Luthi, H.U. Gudel, M.P. Hehlen  
Phys. Rev. B, 61 (2000), p. 3337
- [25] H. Wang, M. Yu, C.K. Lin, J. Lin  
J. Colloid Interface Sci., 300 (2006), p. 176

- [26] M. Yu, J. Lin, J. Fang  
Chem. Mater., 17 (2005), p. 1783
- [27] Y. Cui, X. Fan, Z. Hong, M. Wang  
J. Nanosci. Nanotechnol., 6 (2006), p. 830
- [28] K.W. Kramer, D. Biner, G. Frei, H.U. Gudel, M.P. Hehlen, S.R. Luthi  
Chem. Mater., 16 (2004), p. 1244
- [29] S. Xu, D. Fang, Z. Zhang, Z. Jiang  
J. Solid State Chem., 178 (2005), p. 2159
- [30] G. De, W. Qin, J. Zhang, J. Zhang, Y. Wang, C. Cao, Y. Cui  
Solid State Commun., 137 (2006), p. 483
- [31] H. Schäfer, P. Ptacek, K. Kömpe, M. Haase  
Chem. Mater., 19 (2007), p. 1396
- [32] J.A. Capobianco, F. Vetrone, J.C. Boyer, A. Speghini, M. Bettinelli  
J. Phys. Chem. B, 106 (2002), p. 1181
- [33] M.D. Shinn, W.A. Sibley, M.G. Drexhage, R.N. Brown  
Phys. Rev. B, 27 (1983), p. 6635
- [34] P. Kabro, J.A. Capobianco, F.S. Ermeneux, R. Moncorgé, M. Bettinelli, E. Cavalli  
J. Appl. Phys., 82 (1997), p. 3983
- [35] T. Tsuboi  
Physica B, 293 (2000), p. 84
- [36] J.A. Capobianco, P. Kabro, F.S. Ermeneux, R. Moncorgé, M. Bettinelli, E. Cavalli  
Chem. Phys., 214 (1997), p. 329
- [37] R.E. Di Paolo, E. Cantelar, X.M. Wang, T. Tsuboi, F. Cussó  
J. Phys. Condens. Matter, 13 (2001), p. 7999

**Table 1.** Nominal and measured atomic Si/V ratios and crystallite size of the SiO<sub>2</sub>-Ln:YVO<sub>4</sub> composite samples.

	Treatment	Si/V nominal	Si/V XPS	Crystallite size (nm)
Sample DC	As prepared	1	2.40	26
Sample UC	As prepared	1	2.38	26
	1000 ° C	1	3.05	30

## Figure Captions

**Figure 1.** SEM micrograph (magnification bar = 50  $\mu$  m) and TEM micrograph (inset) of sample DC.

**Figure 2.** EDX spectra for sample DC as prepared and sample UC, as prepared and calcined at 1000 ° C. The most intense peaks corresponding to each element have been labelled.

**Figure 3.** XRD patterns for sample DC as prepared and sample UC, as prepared and calcined at different temperatures.

**Figure 4.** IR spectra for samples DC and UC, as prepared.

**Figure 5.** Emission (top) and excitation (down) spectra for sample DC.

**Figure 6.** Colour coordinates for sample DC as prepared and sample UC calcined at 1000 ° C.

**Figure 7.** UC emission spectra for sample UC, as prepared and calcined at different temperatures (  $\lambda$  ex = 980 nm).

**Figure 8.** SEM micrograph for sample UC calcined at different temperatures (magnification bar = 20  $\mu$  m).

**Figure 9.** Partial energy level diagram of Yb<sup>3+</sup> and Er<sup>3+</sup> ions showing (a) up-conversion energy transfer mechanisms following Yb<sup>3+</sup> excitation and (b) back-transfer from Er<sup>3+</sup> to Yb<sup>3+</sup> following the excitation of the upper Er<sup>3+</sup> multiplets.

**Figure 10.** Power dependence of the up-converted luminescence of Er<sup>3+</sup> after pumping to the Yb<sup>3+</sup> ions. It follows an approximate quadratic dependence as expected from the required two photon excitation.

**Figure 11.** DTA curve obtained for sample UC.

**Figure 12.** Decay time of the Er<sup>3+</sup> green emission, after pulsed excitation to the emitting multiplets (2H<sub>11/2</sub>, 4S<sub>3/2</sub>), for samples calcinated at different temperatures.

Figure 1

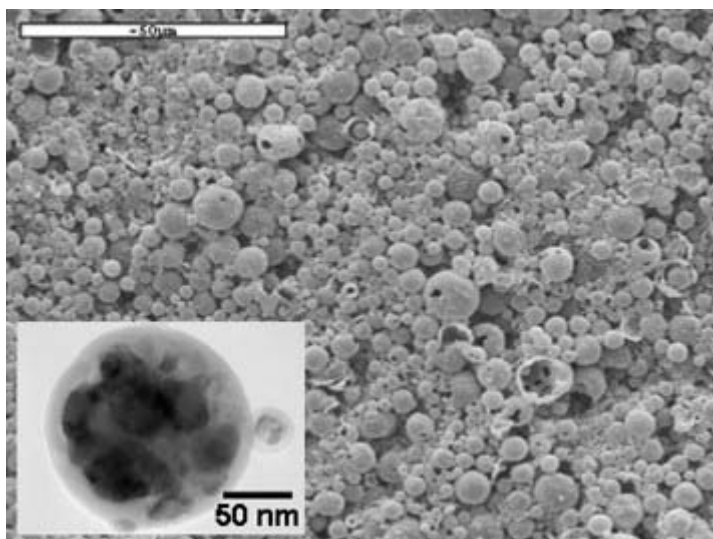


Figure 2

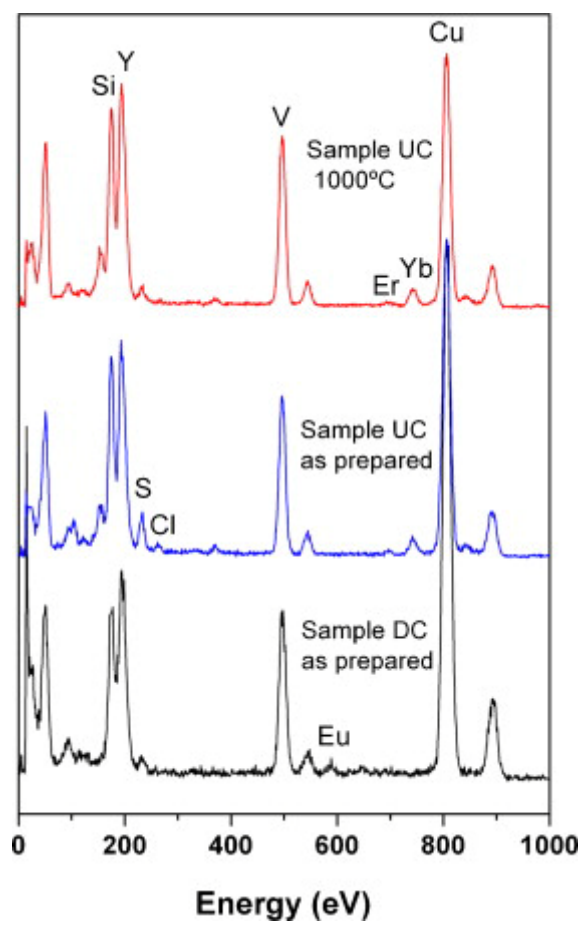


Figure 3

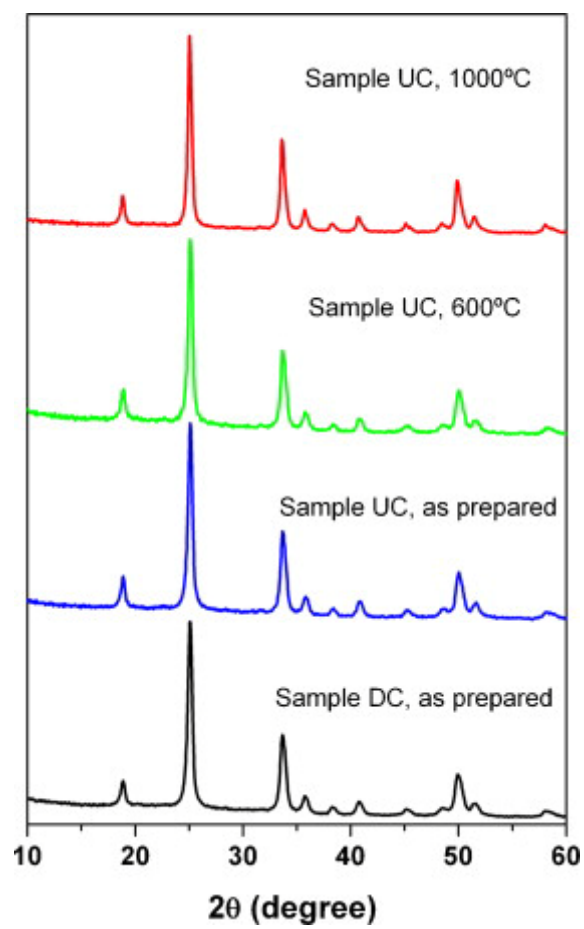




Figure 4

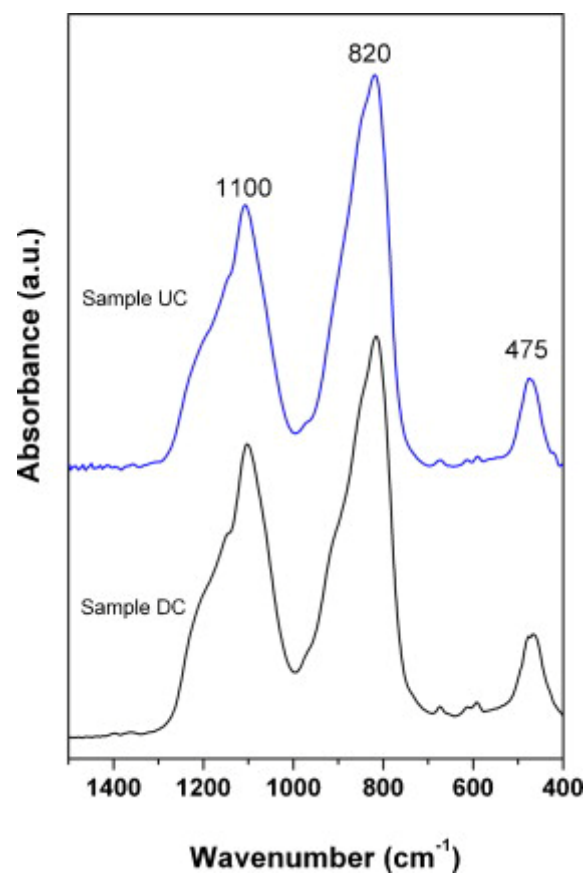


Figure 5

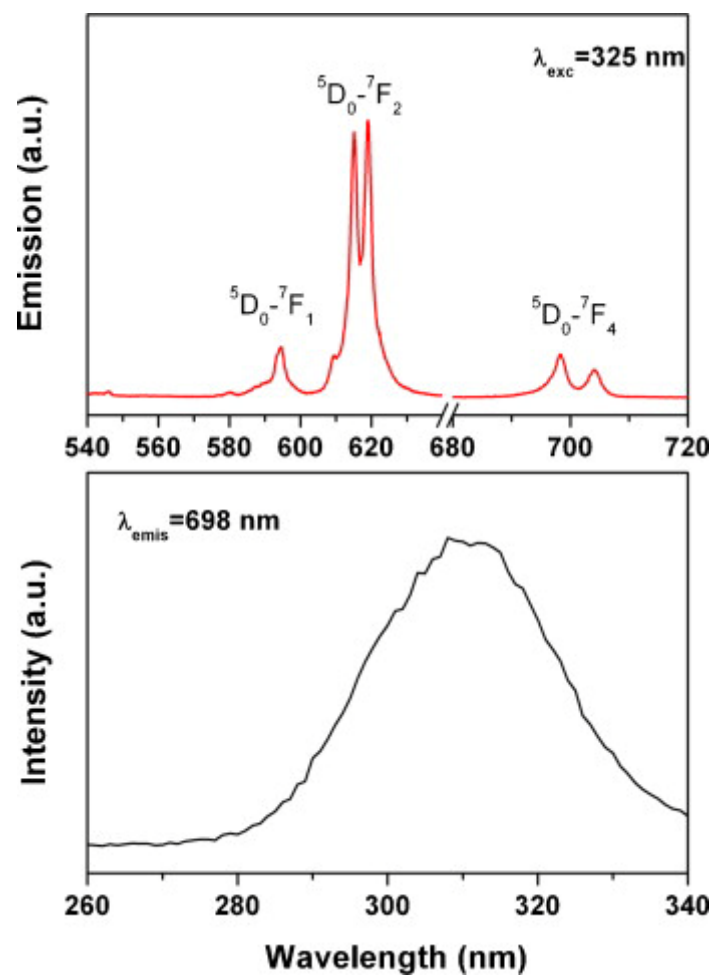


Figure 6

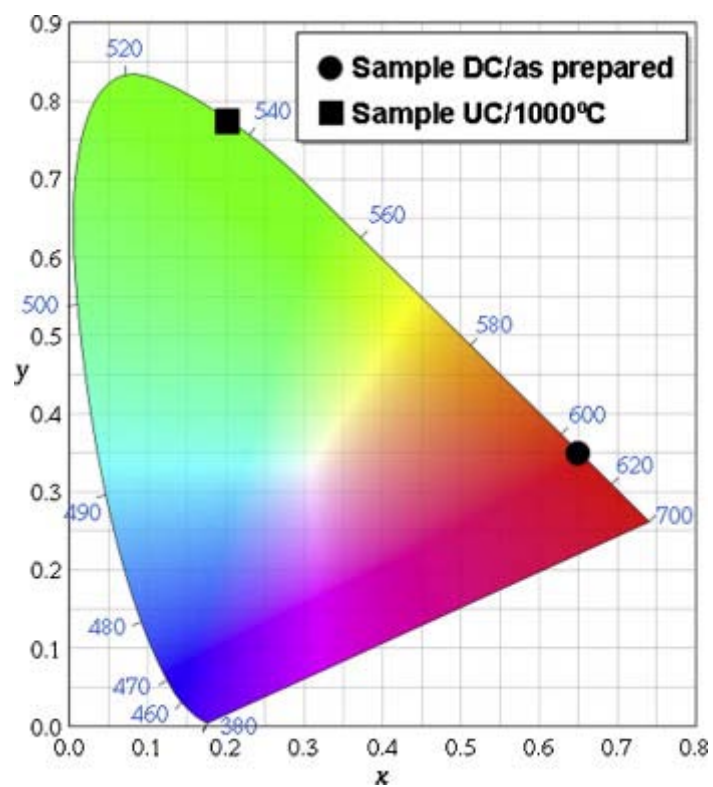


Figure 7

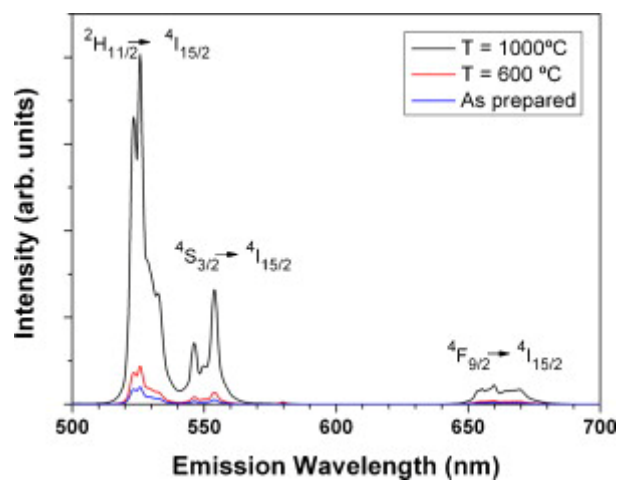


Figure 8

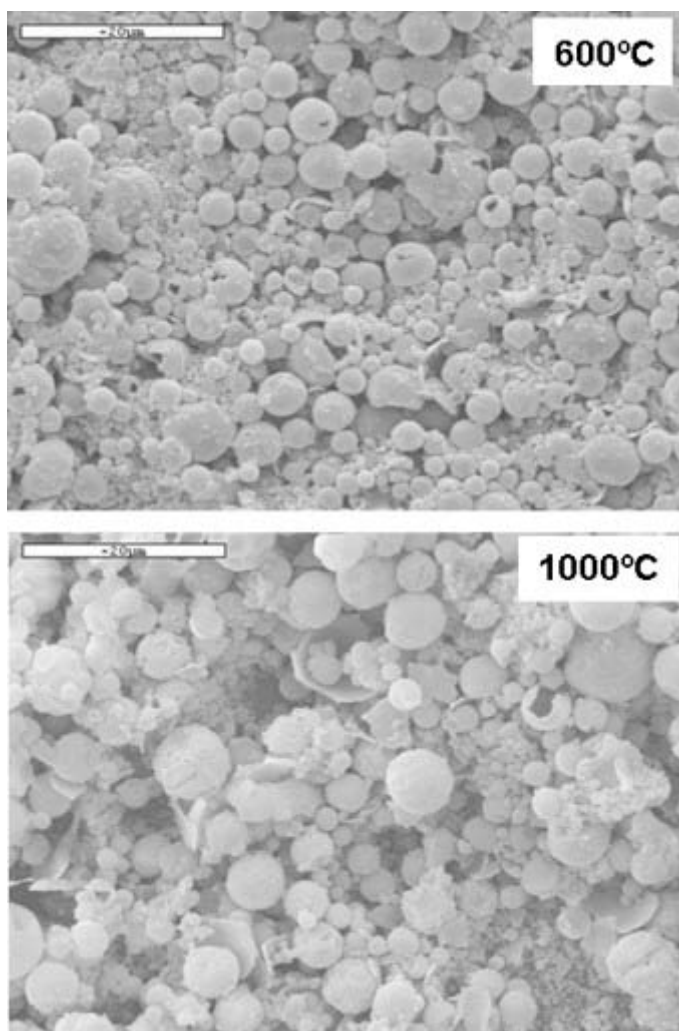


Figure 9

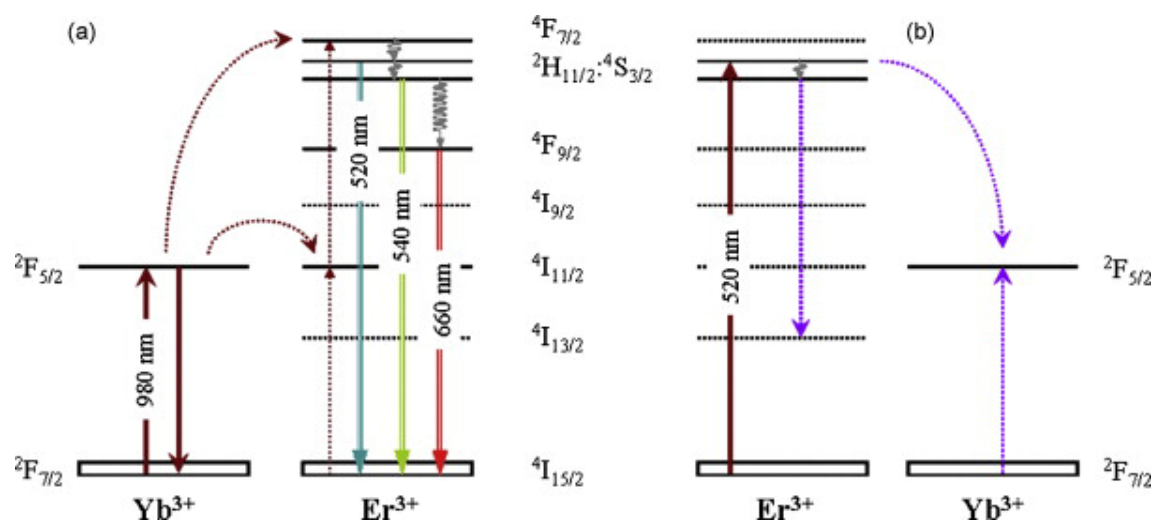


Figure 10

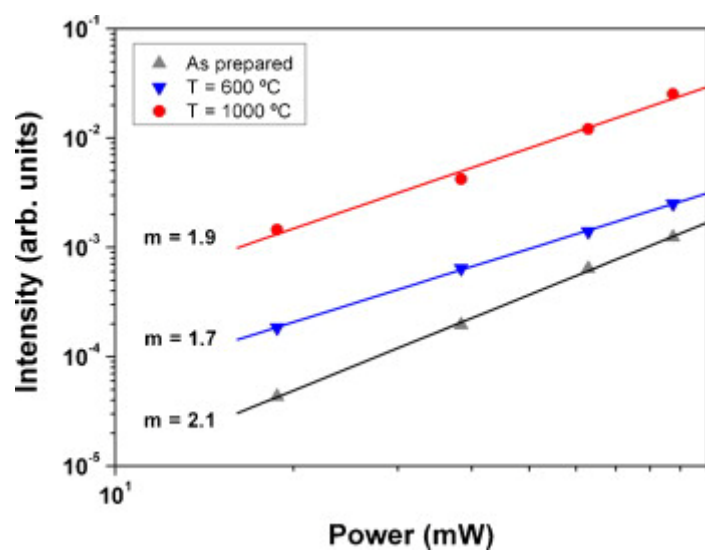


Figure 11

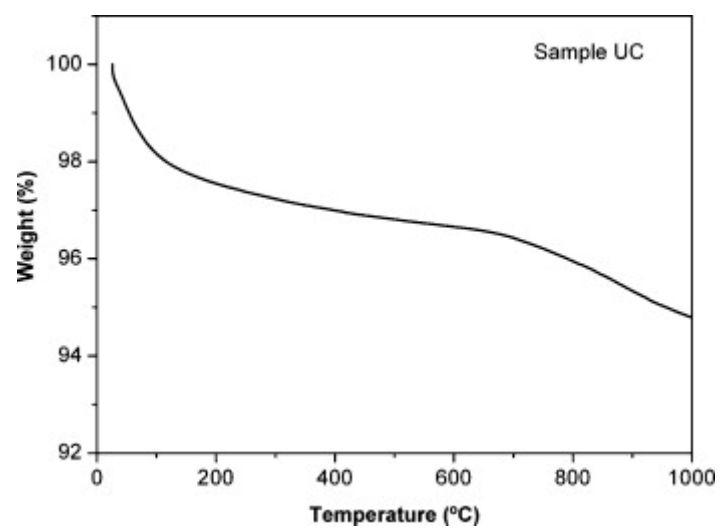




Figure 12

